Polymer 50 (2009) 2281–2289

Contents lists available at ScienceDirect

Polymer

journal homepage: www.elsevier.com/locate/polymer

Electrospinning of L-tyrosine polyurethanes for potential biomedical applications

Parth N. Shah [a], Rachel L. Manthe [b], Stephanie T. Lopina [a,b], Yang H. Yun [b,*]

[a] Department of Chemical & Biomolecular Engineering, The University of Akron, Whitby Hall, Akron, OH 44325, USA
[b] Department of Biomedical Engineering, The University of Akron, Sidney Olson Research Center, Akron, OH 44325, USA

ARTICLE INFO

Article history:
Received 8 December 2008
Received in revised form
16 February 2009
Accepted 22 February 2009
Available online 19 March 2009

Keywords:
Biodegradable polyurethanes
Electrospinning
Nanofibers

ABSTRACT

Biodegradable segmented L-tyrosine polyurethanes (LTUs) have been developed using a tyrosine based chain extender desaminotyrosine-tyrosyl-hexyl ester (DTH). Two such biodegradable LTUs, polycaprolactone diol-hexamethylene diisocyanate-desaminotyrosine-tyrosyl-hexyl-ester (PCL-*L*-DTH) and polycaprolactone diol-4,4′-methylenebis(cyclohexyl isocyanate)-desaminotyrosine-tyrosyl-hexyl-ester (PCL-*C*-DTH), have been electrospun, and the effect of solution concentration on the membrane properties has been examined. Scanning electron microscopy (SEM) images show that fiber diameter and structural morphology of the electrospun LTU membranes are a function of the polymer solution concentration. It has been observed all concentrations of PCL-*L*-DTH lead to the formation of beaded nanofibers; whereas, PCL-*C*-DTH polyurethane leads to the formation of non-beaded fibers with diameters in the micrometer range. Furthermore, the average fiber diameter enlarges with an increase in the polymer solution concentration. Hydrolytic degradation studies show similar mass loss profiles for both PCL-*L*-DTH and PCL-*C*-DTH polyurethane membranes over a period of 28 days. However, the loss of structure and morphology is more readily observed in the case of PCL-*L*-DTH membranes. Based on the results obtained from this investigation, the electrospun non-woven LTU membranes show excellent potential for biomedical applications such as formulation of drug/gene delivery devices and tissue engineering scaffolds.

© 2009 Elsevier Ltd. All rights reserved.

1. Introduction

Segmented polyurethane elastomers have been used as biomaterials for several decades due to their unique physico-mechanical properties and favorable biocompatibility [1]. Specifically, polyurethanes have been used in implantable devices such as insulators for cardiac pacing leads, ventricular assist devices, vascular prostheses, breast implant coatings, tissue adhesives, skin wound dressings, and etc. [2–4]. A majority of the biomedical applications, to date, require the use of biostable polyurethanes, and the primary focus of development has been upon non-degradable formulations. However, a number of implantable devices such as cardiovascular implants [5,6], artificial skin [2,7], cancellous bone graft substitutes [8,9], and nerve conduits [10], would benefit with elastomeric biodegradable polyurethanes.

Unfortunately, the development of segmented biodegradable biomedical polyurethanes has received relatively little interest. The degradation mechanisms of these polyurethanes can be generally classified as hydrolytic, oxidative, and enzymatic. Hydrolytically degradable polyurethanes have been synthesized by the incorporation of soft segments such as polyhydroxyacids, polyesters, etc. [10–16]; whereas, the use of polyether based soft segment molecules such as poly(ethylene glycol) (PEG) or poly(tetramethylene oxide) (PTMO) can make the polyurethane susceptible to oxidative degradation [16–19]. The urethane, ester, and amide bonds within the hard segments also show some susceptibility towards simple chemical hydrolysis, but enzymatic degradation of these moieties is minimal due to the absence of conformationally specific sequences required for enzyme–substrate cleavage interactions [16]. To increase the responsiveness of polyurethanes towards enzymatic degradation, Woodhouse et al. have introduced an L-phenylalanine derived chain extender within the polyurethane backbone [20,21].

We have also developed elastomeric biodegradable segmented amino acid based polyurethanes by the structural modification of poly(L-tyrosine). In developing these molecules, we have introduced functionalities into the polymeric backbone to make them susceptible to both hydrolytic and enzymatic degradation mechanisms. Two such polyurethanes have been synthesized. The common components are poly(ε-caprolactone) (PCL) as the resorbable soft segment diol and DTH as the degradable hard segment chain extender. The material properties of the LTUs can be

* Corresponding author. Tel.: +1 330 972 6619; fax: +1 330 374 8834.
E-mail address: yy@uakron.edu (Y.H. Yun).

0032-3861/$ – see front matter © 2009 Elsevier Ltd. All rights reserved.
doi:10.1016/j.polymer.2009.02.048

tuned by choosing either 1,6-diisocyanatohexane or 4,4′-methylenebis(cyclohexyl isocyanate) as the hard segment diisocyanate [22].

Diphenolic DTH monomer has been synthesized by a carbodiimide mediated amide bond formation between L-tyrosine and a derivative of L-tyrosine that is a structural analog of L-dopa. Since, the polyurethane synthesis is carried out using the terminal hydroxyl groups of DTH, the amino acids are introduced into the polymer backbone rather than as pendant side chains, as is the case with polyurethanes developed by Woodhouse et al. This difference in the chemical structure is expected to have an effect on the degradation rates of the polyurethanes. Investigation of the material properties of LTUs indicates that they possess mechanical properties comparable to soft tissues (e.g. skin, artery, and articular cartilage) [23]. Hence, an ideal application for these polyurethanes would be as scaffolds for soft tissue engineering since these materials exhibit elasticity and malleability [24]. Additionally, Gogolewski et al. have shown that biodegradable polyurethane scaffolds can withstand the action of high stresses and undergo an elastic recovery with little or no hysteresis [10]. Furthermore, LTUs offer a wide range of material properties that may be easily tuned by changing the polymer structure [23].

Numerous studies suggest that the design of an appropriate scaffold is crucial for successful tissue engineering [25–27]. Reneker et al. state that ideal scaffolds must satisfy a number of often conflicting demands including an appropriate level and size of porosity allowing for cell migration, sufficient surface area, a variety of surface chemistries that encourage cell adhesion, growth, migration, and differentiation, and a degradation rate that closely matches regeneration rate of the desired natural tissue [27]. Additionally, scaffolds must mimic the structure of the natural extracellular matrix to achieve an optimal outcome in generating functional tissues [26]. While numerous techniques for the fabrication of tissue engineering matrices exist, electrospun matrices are of special interest since this technique results in non-woven fabrics with micron to sub-micron sized diameters with topology that mimicks the native extracellular matrix (ECM) [28].

We have also found that electrospinning of biodegradable polyurethanes for fabrication of tissue engineering scaffolds has received little attention. This lack of information coupled with the excellent material properties of LTUs has prompted us to investigate the electrospinning of our biomaterials. Consequently, the effects of polymer solution concentrations of PCL-*L*-DTH and PCL-*C*-DTH upon the fiber properties have been investigated. We hypothesize that by varying the polymer solution concentrations while keeping the other electrospinning parameters constant, the fiber diameter and morphology can be varied. In addition, the swelling properties and the degradation kinetics of the electrospun membranes have also been investigated and correlated to the solution concentrations. Thus, the primary purpose of this study is to electrospin nanoporous tissue engineering scaffolds using LTUs and characterize them for properties pertaining to biomedical applications.

2. Methods and materials

2.1. Materials

L-Tyrosine, *n*-hexanol, diethyl ether, phloretic acid (also known as desaminotyrosine or DAT), *N*-ethyl-*N*′-dimethylaminopropyl carbodiimide hydrochloride (EDC·HCl), 4-dimethylaminopyridine (DMAP), dichloromethane (DCM), tetrahydrofuran (THF), dimethylformamide (DMF), polycaprolactone diol (PCL1250) (M.W. 1250), 1,6-diisocyanatohexane (HDI), 4,4′-methylenebis(cyclohexyl isocyanate) (HMDI), magnesium sulfate ($MgSO_4$), stannous octoate and hydrochloric acid (HCl) were obtained from Sigma–Aldrich Corporation (St. Louis, MO). All the above chemicals except for dichloromethane and dimethylformamide were used without further purification. Dichloromethane was dehydrated by distillation with anhydrous calcium hydride to remove traces of moisture prior to each reaction step. Dimethylformamide was dehydrated with anhydrous calcium hydride and filtered prior to the reaction step. 1,1,1,3,3,3 hexafluoro-2-propanol (HFIP) was obtained from VWR International (Bridgeport, NJ) and used as obtained.

2.2. Synthesis of L-tyrosine polyurethanes

The monomer DTH, was synthesized according to the protocol developed by Sen Gupta et al. [29,30]. Two forms of biodegradable polyurethanes were synthesized according to Sarkar et al.'s protocol [22,31]. Since 1,6-diisocyanatohexane has a linear structure, we will be using "*L*" for this diisocyanate. In contrast, 4,4′-methylenebis(cyclohexyl isocyanate) has two cyclohexyl rings and therefore we will be using "*C*" for this diisocyanate. The structures of the PCL-*C*-DTH and PCL-*L*-DTH are shown in Fig. 1.

2.3. Electrospinning of PCL-based biodegradable polyurethanes

Electrospinning of PCL-*C*-DTH and PCL-*L*-DTH was attempted using a single solvent system by dissolving the polymers into

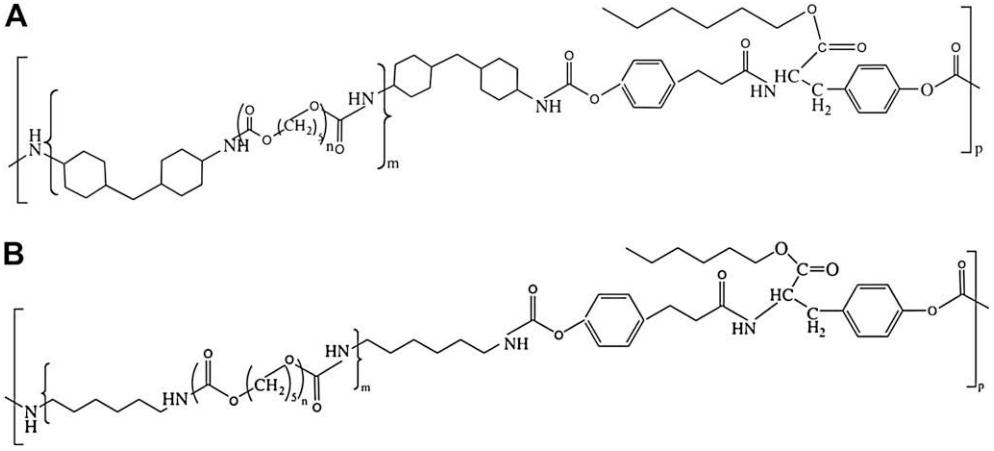

Fig. 1. Chemical structures of L-tyrosine based polyurethanes (A) PCL-*C*-DTH (B) PCL-*L*-DTH.

1,1,1,3,3,3-hexafluoro-2-propanol (HFIP) at concentrations of 10, 15, 20 and 25% (w/v). The polymeric solution was loaded in a 3 ml syringe (National Scientific, Rockwood, TN) connected to an 18-gage blunt tip needle using a Tygon tubing (Saint Gobain Performance Plastics, Akron, OH). The needle was connected to a high voltage power supply and the ground electrode was connected to the collection plate. Each of the polymer solution mentioned above was spun using a gap distance of 17 cm. The voltage was changed from 0 to 30 kV until the formation of a stable Taylor cone. The processing parameters used for the electrospinning process are summarized in Table 1.

2.4. Scanning electron microscopy (SEM)

The surface morphology of the electrospun membranes was assessed using a Hitachi S-2150 SEM. The electrospun membranes were placed on aluminum stubs using a double stick carbon tape and sputter coated with a very thin layer of silver/palladium (Emitech). The morphological features were observed at an accelerating voltage of 20–25 kV under high vacuum. The images were captured using the Quartz PCI system.

2.5. Determination of fiber diameters

The diameters of the electrospun fibers were measured using the images obtained from scanning electron microscopy. Three samples were imaged for each solution concentration and for each polymer. For all samples, images were analyzed using Zeiss Axiovision LE 4.6 (Carl Zeiss) by setting up an appropriate scaling factor. A total of 450 fibers per sample concentration were analyzed, and the mean fiber diameters as well as the fiber diameter distributions were determined.

2.6. Swelling studies of electrospun membranes

Electrospun films were cut into dimensions of 2×2 cm and weighed to an accuracy of 0.1 mg on an analytical balance (Excellence Level, Mettler Toledo, Columbus, OH). The specimens were placed in closed containers containing 10 ml of sterile phosphate buffered saline (PBS, pH 7.4) and incubated at 37 °C. At pre-determined intervals of time, the specimens were retrieved, dried to remove any surface moisture, and weighed. The weights of the incubated samples were compared to their initial values to obtain the swelling ratios. Three replicates per sample type were used for swelling studies.

2.7. Mass loss of electrospun membranes

Samples were prepared according to Section 2.6, and the degradation studies were performed using sterile PBS (pH 7.4). Each sample was placed into an individual vial containing 10 ml of sterile PBS and incubated at 37 °C. Samples of each membrane type ($n = 3$) were removed from the buffer on days 1, 3, 7, 10, 14, 21, and 28. After drying the samples in a vacuum oven at 37 °C for 48 h, the samples were reweighed. The percent of the total mass loss was calculated as described by Wagner et al. [20]. The samples were then analyzed using SEM to determine the surface morphology as described in Section 2.4.

Table 1
Processing parameters of PCL-*L*-DTH and PCL-*C*-DTH polyurethanes.

Polymer Type	Concentration (% w/v) in HFIP	Volumetric flow rate (ml/min)	Electric potential (kV/cm)	Average fiber diameter (nm)
PCL-*L*-DTH	15	0.035	1.364	870 ± 12
	20	0.035	1.364	890 ± 35
	25	0.035	1.364	930 ± 15
PCL-*C*-DTH	10	0.035	1.364	1201 ± 143
	15	0.035	1.364	2324 ± 83
	20	0.035	1.364	2596 ± 267

2.8. Statistical analysis

The significance of varying the polymer concentration upon the average fiber diameter and the swelling and degradative properties of the membranes were determined using ANOVA and Tukey–Kramer post-hoc test. Electrospun membranes formulated using different concentrations of PCL-*L*-DTH and PCL-*C*-DTH were compared to each other. Statistical analysis software package SAS for Windows (Cary, NC, USA) was used for data analysis. All data has been expressed as mean ± standard error of the mean (S.E.), and the data was considered statistically significantly different when p-value < 0.05.

3. Results

3.1. Morphology of electrospun scaffolds

Fibrous membranes have been obtained by electrospinning PCL-*L*-DTH or PCL-*C*-DTH solutions in HFIP at pre-determined processing conditions (Table 1). The concentrations of the polymers have been varied in order to study their role on the membrane properties. All electrospun membranes fabricated using PCL-*C*-DTH and PCL-*L*-DTH polymers are white in appearance. The morphology of electrospun polymeric scaffolds at all polymer concentrations demonstrates a porous structure comprised of randomly oriented non-woven fibers of variable sub-micron to micron diameters (Fig. 2).

Fig. 2A–C illustrates a representative sample of the morphologies obtained for membranes spun using different concentrations of PCL-*L*-DTH. SEM images show that all PCL-*L*-DTH polymer concentrations lead to the formation of beaded fibers. At a concentration of 15% (w/v), nanofibers with beads on a string morphology are observed. Furthermore, these beads are found to fuse together and solidify into larger molten structures that are randomly dispersed throughout the membrane. Increasing the polymer concentration to 20% (w/v) leads to the formation of fibers with the most consistent structure and minimum amount of beads. A further increase in the polymer concentration to 25% (w/v) displays thicker fibers as well as molten fibrous aggregates. Interestingly, a higher degree of bead formation is observed compared to the fibers for 20% (w/v) polymer membranes. The degree of bead formation shows an interesting pattern where bead formation decreases as the PCL-*L*-DTH concentration increases from 15 to 20%, but increases as the PCL-*L*-DTH concentration is increased to 25% (w/v). In contrast, electrospinning of PCL-*C*-DTH polymer leads to the formation of micron sized fibers with a smooth surface morphology and without the presence of any type of beaded structure (Fig. 2D–F). This morphology is preserved upon increasing the polymer concentration from 10% to 20%; however, thicker fibers are obtained.

3.2. Fiber diameter distribution of electrospun scaffolds

Fig. 3A–C depicts the typical fiber diameter distributions obtained for electrospun membranes formulated using various concentrations of PCL-*L*-DTH solutions. The fibers for 15% concentration show a tight fiber diameter distribution with majority of the fibers having diameters between 400 and 1200 nm and an average fiber diameter of 870 ± 12 nm (Fig. 3A). Fibers for 20%

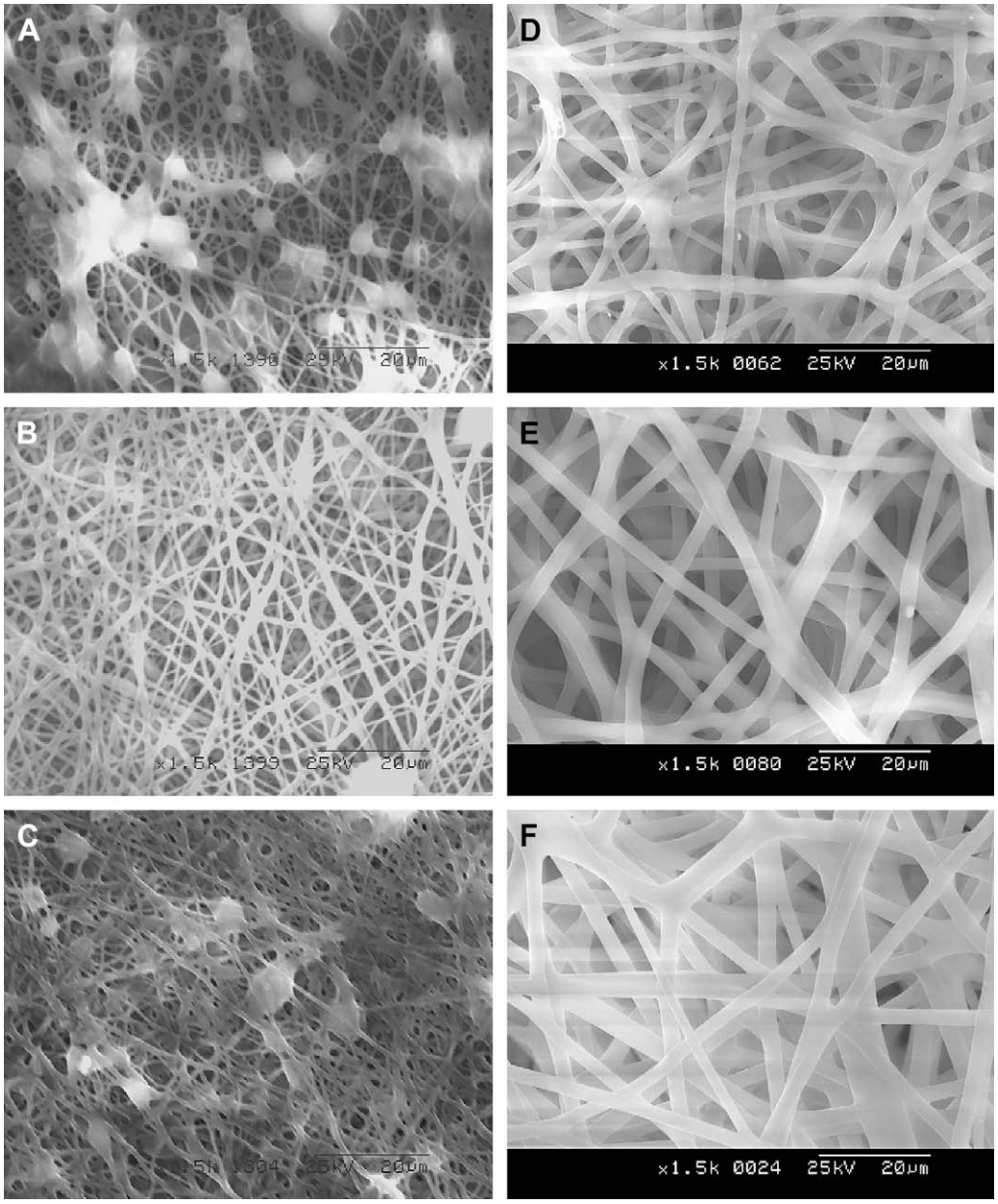

Fig. 2. SEM micrographs of electrospun membranes obtained by using PCL-*L*-DTH solution (A) 15% (w/v) solution (B) 20% (w/v) solution, and (C) 25% (w/v) solution and PCL-*C*-DTH solution (D) 10% (w/v) solution (E) 15% (w/v) solution, and (F) 20% (w/v) solution.

concentration range between 400 and 1500 nm with an average fiber diameter of 890 ± 35 nm (Fig. 3B). Increasing the polymer concentration to 25% leads to the formation of fibers with diameters ranging from 400 to 1600 nm and an average fiber diameter of 930 ± 15 nm.

Typical fiber diameter distributions arising from electrospinning of various concentrations of PCL-*C*-DTH polyurethane solutions have been shown in Fig. 4A–C. Electrospinning of 10% (w/v) PCL-*C*-DTH polyurethane leads to fibers having diameters between 400 and 2200 nm with an average fiber diameter of 1201 ± 143 nm (Fig. 4A). In the case of the 15% (w/v) PCL-*C*-DTH solution, fiber diameters ranged from 1400 to 3200 nm with an average fiber diameter of 2324 ± 83 nm (Fig. 4B). A further increase in solution concentration to 20% (w/v) PCL-*C*-DTH, slightly increases the mean fiber diameter (2596 ± 267 nm) with a range between 1400 and 3800 nm.

3.3. Correlation of fiber diameters and polymer solution concentration

A correlation between average fiber diameter and PCL-*L*-DTH concentration used for electrospinning (Fig. 3A–C) shows that the fiber diameter distribution shifts towards larger sizes with increasing polymer concentrations. Although, the average fiber diameter increases almost linearly with an increase in the PCL-*L*-DTH concentration in HFIP, statistical analysis shows no significant differences with polymer concentrations (p =1.000 for 15 and 20% concentrations, p = 0.9991 for 15 and 25% concentrations, and p = 0.992 for 20 and 25% concentrations).

The correlation between polymer solution concentration and average fiber diameter (Fig. 4A–C) shows results similar to those for PCL-*L*-DTH where the average fiber diameter increases with increasing polymer concentration. A sharper rise in the average

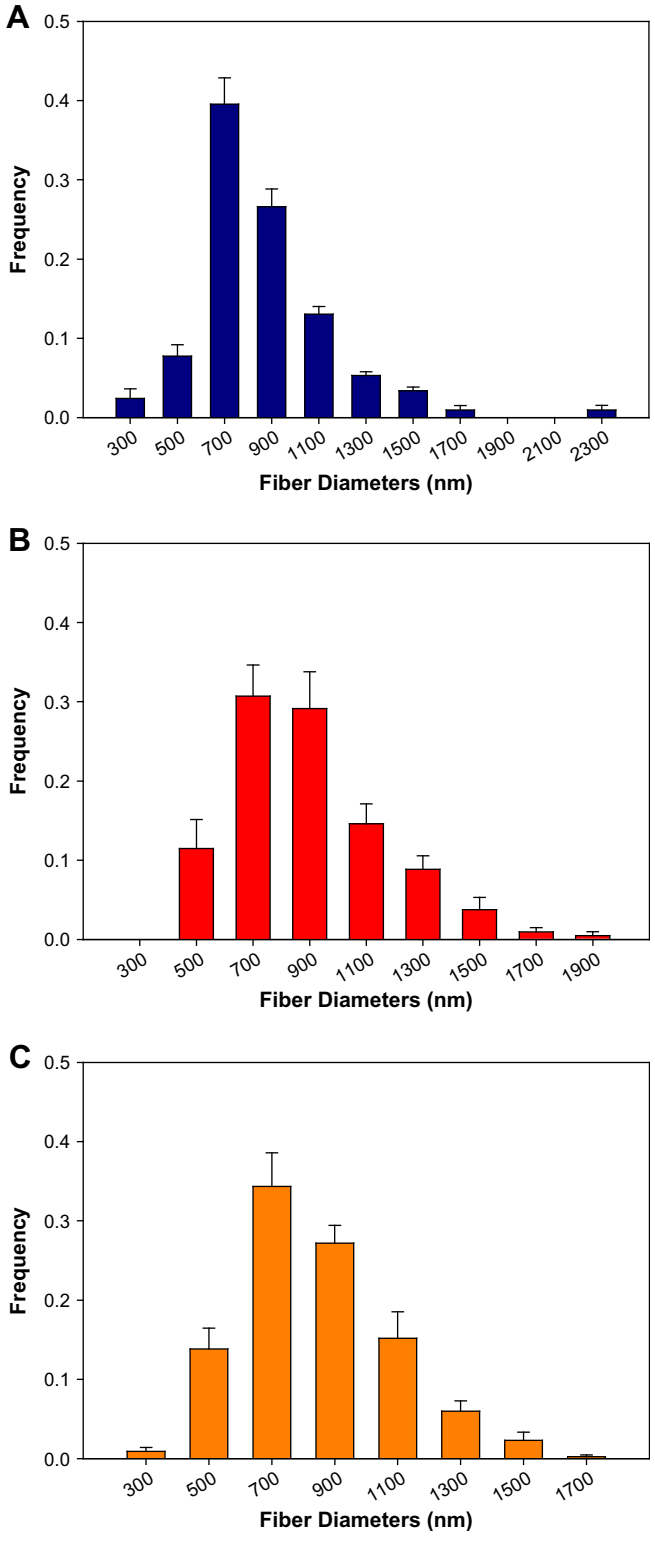

Fig. 3. Fiber diameter distribution of PCL-*L*-DTH electrospun membranes based on SEM micrographs (A) 15% (w/v) solution (B) 20% (w/v) solution, and (C) 25% (w/v) solution.

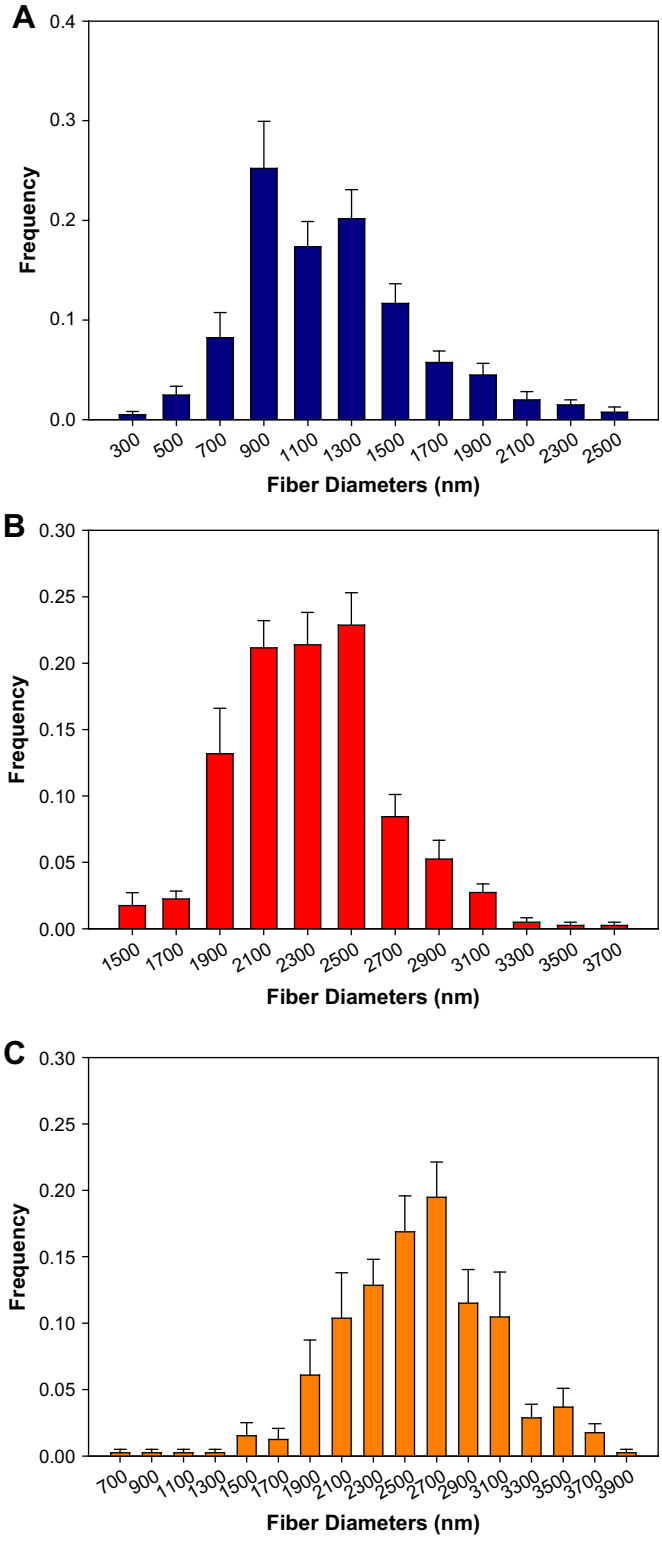

Fig. 4. Fiber diameter distribution of PCL-*C*-DTH electrospun membranes based on SEM micrographs (A) 10% (w/v) solution (B) 15% (w/v) solution, and (C) 20% (w/v) solution.

fiber diameter is also observed upon increasing the concentration from 10 to 15% (w/v). Unlike the PCL-*L*-DTH membranes, the average fiber diameters obtained for PCL-*C*-DTH membranes at each investigated concentrations are statistically different from each other ($p < 0.001$ for 10 and 15% concentrations, $p = 0.0119$ for 15 and 20% concentrations, and $p < 0.001$ for 10 and 20% concentrations).

Thus, the primary difference between the results shown in Figs. 3 and 4 is that electrospinning of PCL-*C*-DTH leads to the formation of micron sized fibers. In contrast, the electrospinning of PCL-*L*-DTH

leads to nanofibers. Furthermore, the polymer concentration has a statistically significant impact on the average fiber diameters in the case of PCL-*C*-DTH membranes.

3.4. Swelling characteristics of electrospun membranes

The water absorption kinetics of PCL-*L*-DTH and PCL-*C*-DTH electrospun membranes are shown in Fig. 5A and B. For each of the PCL-*L*-DTH electrospun membranes, the water absorption continues to increase until equilibrium is reached (approximately 24 h of incubation). At equilibrium, the swelling ratios for 15, 20 and 25% PCL-*L*-DTH membranes are 1.730 ± 0.125, 1.894 ± 0.075, 2.135 ± 0.139, respectively. At 24 h, the swelling ratios for 10, 15 and 20% PCL-*C*-DTH membranes are 1.937 ± 0.010, 1.216 ± 0.038, 1.340 ± 0.035, respectively. Fig. 5A shows that an increase in the PCL-*L*-DTH concentration leads to an increase in the water absorption by the membranes. However, statistical analysis of the swelling data does not reveal any significant differences between the water uptake at equilibrium for PCL-*L*-DTH membranes ($p = 0.9996$ for 15 and 20% membranes, $p = 0.561$ for 15 and 25% membranes, and $p = 0.9802$ for 20 and 25% membranes).

In the case of PCL-*C*-DTH electrospun membranes, increasing amount of water absorption occurs until equilibrium is reached at 24 h (Fig. 5B). Afterwards, extremely small incremental changes occur in the swelling ratio. In contrast to the results obtained for PCL-*L*-DTH membranes, the maximum degree of swelling is observed for the 10% electrospun membranes when they are formulated using PCL-*C*-DTH. Furthermore, statistical analysis of PCL-*C*-DTH membrane swelling data shows a significantly higher water uptake for 10% membranes at all time points after 3 h (all p-values < 0.0001) in comparison to the 15 and 20% membranes. However, no statistically significant differences exist between the swelling ratios for 15 and 20% membranes at any time point.

3.5. Hydrolytic degradation of electrospun membranes

The mass loss profiles for 15, 20 and 25% (w/w) PCL-*L*-DTH electrospun membranes presented in Fig. 6A show that the initial degradation rates for all membranes are similar; however, the 25% membrane seems to retain marginally more mass compared to the 15 and 20% membranes at the end-point for the degradation studies (28 days). Statistical analysis of the degradation data shows significant differences between the masses retained by the 25% membrane and 15% on day 21 ($p = 0.0135$). By the 28th day of degradation, no statistically significant differences exist among the masses retained by either type of membrane ($p = 1.000$ for comparison of 15 and 20% membranes, $p = 0.0747$ for the comparison of 15 and 25% membranes, and $p = 0.1501$ for the

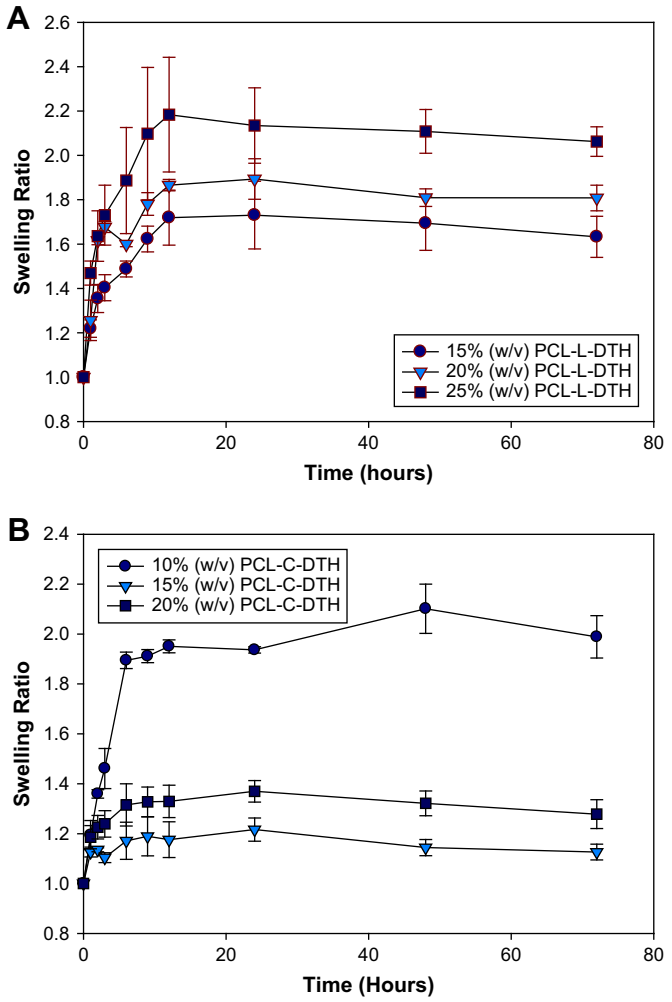

Fig. 5. Dynamic swelling characteristics of electrospun membranes (A) PCL-*L*-DTH polyurethane (B) PCL-*C*-DTH polyurethane. Data represented as mean ± standard error for $n = 3$.

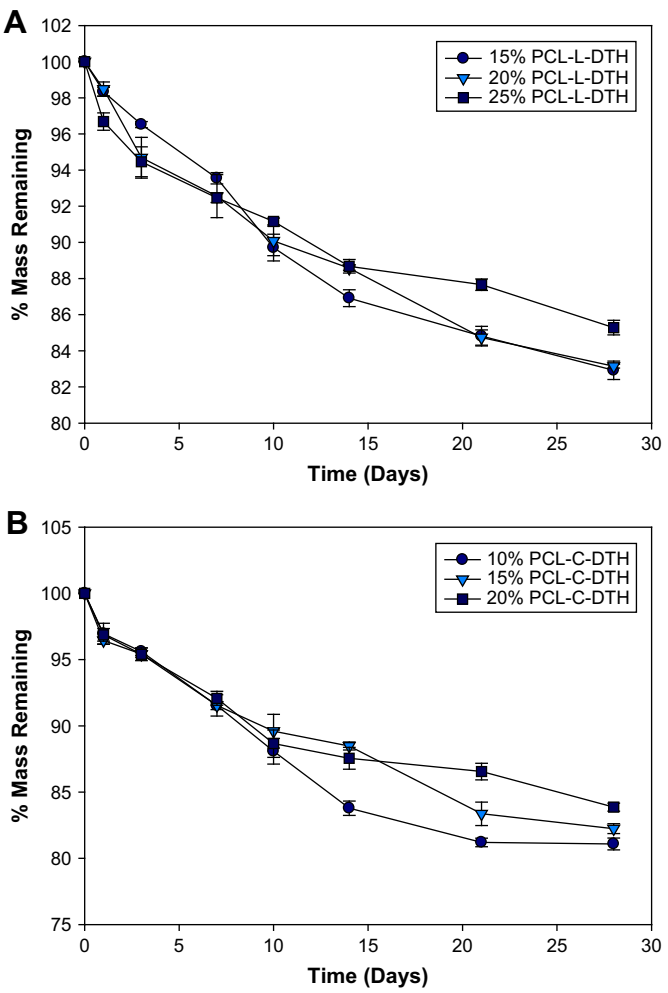

Fig. 6. Hydrolytic degradation of electrospun membranes over a period of 28 days (A) PCL-*L*-DTH polyurethane (B) PCL-*C*-DTH polyurethane. Data represented as mean ± standard error for $n = 3$.

comparison of 20 and 25% membranes). Similar results are also observed for the PCL-*C*-DTH membranes (Fig. 6B) where the 20% membrane retains a slightly higher mass compared to 10 and 15% membranes after 28 days of *in vitro* hydrolytic degradation. These differences are not statistically different.

After hydrolytic degradation for 28 days, the structure and morphology of the electrospun membranes is examined by SEM to observe morphological changes occurring in the membranes with mass loss. As seen from the SEM micrographs (Fig. 7A–C), the effects of hydrolytic degradation on electrospun membranes fabricated using polymer solutions of different concentrations are varied. After 4 weeks of incubation in PBS, the interconnected void structure in the 15% polymer membrane has been completely degraded, and the fiber-bonding points are found to be fused together giving rise to a continuous molten structure with a few randomly interspersed fibers. The presence of beaded molten structures is also observed in the case of the degraded 20% polymer membrane; however, the bead formation is observed to occur to a lesser extent than in the case of the 15% polymer membrane. Also, the fibrous structure of the membrane is not completely lost but appears as if the adjacent fibers have fused together to form larger, thicker fibers. In the case of the 25% polymer membrane, the fibrous structure of the membrane is still observed to be intact, and a few beaded or molten structures are observed. Further, the edges of the fibers appear frayed, but the thickening of the fibers is not observed.

Noticeable changes are observed in the membranes and in the fiber morphologies upon analysis of the PCL-*C*-DTH membranes

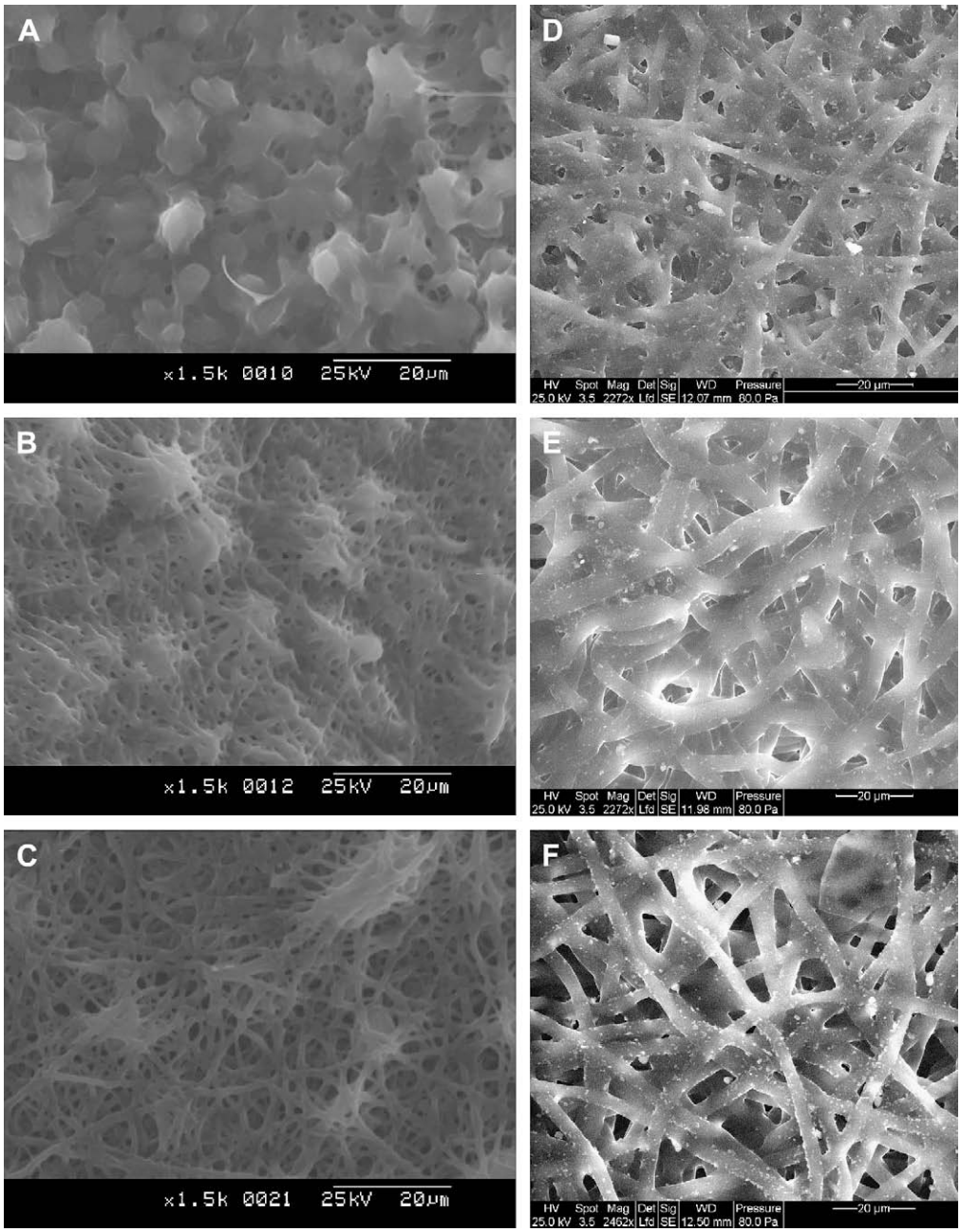

Fig. 7. SEM micrographs of electrospun PCL-*L*-DTH membranes degraded for 28 days (A) 15% (w/v) solution, (B) 20% (w/v) solution, and (C) 25% (w/v) solution and electrospun PCL-*C*-DTH membranes degraded for 28 days (D) 10% (w/v) solution, (E) 15% (w/v) solution, and (F) 20% (w/v) solution.

following hydrolytic degradation for 28 days (Fig. 7D–F). Membranes electrospun using 10% and 15% polymer concentrations mostly exhibit fusion of the individual fibers; however, some retention of the individual fiber structure is still observed. These results are in contrast to the PCL-*L*-DTH membranes where almost a complete loss of fiber structure is observed. Along with the fusion of the individual fibers within the membrane, a corresponding decline in the membrane pores and pore volumes is seen. The fusion of the individual fibers also seems to lead to thickening of the fibers. In the case of the 20% polymer membrane, the majority of the morphological features have been found to remain intact. The fiber structure following degradation is extensively preserved although some fusion of the fibers at the interconnected junctions is present. While the fiber edges appear frayed and show the presence of spiky structures a decrease in the fiber diameter due to erosion is not observed.

4. Discussion

The primary goal of this research is to fabricate nanoporous electrospun scaffolds using biodegradable L-tyrosine polyurethanes for tissue engineering applications. Electrospinning has been chosen as the technique for scaffold fabrication using LTUs due to ease of use, adaptability, and the ability of this technique to yield fibers with a nanosize scale [32]. Additionally, the high surface to volume ratio offered by electrospun fibers provides an opportunity for surface modifications with bioactive molecules, while potentially enhancing mass transport properties, drug loading, and cell adhesion. By controlling fiber orientation, the bulk mechanical properties and the biological response to the scaffold can be controlled [32]. Consequently, we believe that electrospun scaffolds developed with biodegradable polyurethanes have tremendous potential in tissue engineering and drug delivery applications.

In the electrospinning of all LTUs the polymer concentration has been shown to be a determining factor in controlling the fiber morphology and diameter [33–36]. The effect of polymer concentration on the morphology of electrospun membranes has been examined while keeping the other parameters such as applied voltage, volumetric flow rate, gap distance, syringe, and needle configuration constant. Morphological examination of PCL-*L*-DTH membranes predominantly shows the presence of nanofibers at all investigated concentrations. On the other hand, PCL-*C*-DTH membranes exhibit a mix of micro- and nanofibers. The fiber diameters enlarge with increasing polymer concentrations for both LTUs [37]. At higher concentrations, the viscoelastic forces associated with increasing viscosity resist the extension and thinning of the jet thus producing thicker fibers [38]. This phenomenon also explains the micron sized fibers obtained upon electrospinning of PCL-*C*-DTH. Apart from the effects of viscoelastic forces, the evaporation rates of the solution can also have an impact on the fiber diameters [39]. PCL-*C*-DTH solutions exhibit higher viscosities compared to PCL-*L*-DTH solutions and consequently lower solvent evaporation rates. An incomplete removal of the solvent by the time the fiber jet reaches the collection plate can facilitate fiber fusion and thus the formation of microfibers. Bead formation is also observed when using a linear diisocyanate based polyurethane compared to a cyclic diisocyanate based polyurethane, but an investigation into the complex phenomenon of bead formation is beyond the scope of this article.

The swelling of polymers, especially polymer gels, occurs mostly because of the presence of hydrophilic functional groups that are capable of forming hydrogen bonds [40]. Another parameter that plays an important role in swelling is the free volume or porosity of the membranes. Fig. 5A shows electrospun PCL-*L*-DTH membranes increase in mass upon swelling. A simultaneous increase in the dimensions is also observed. A comparison of the swelling kinetics of solvent cast films and electrospun membranes shows a rather rapid uptake of water by the electrospun membranes. At equilibrium (24 h), the water uptake for the electrospun membranes is approximately 75–120%; whereas, solvent cast films (10% w/v) show only a 10–15% increase in mass [23]. The higher degree of water uptake by the fibrous membranes occurs since these membranes are highly porous and offer a large free volume. Furthermore, PCL-*L*-DTH is a hydrophobic material, and the solvent cast films show a minimal amount of water uptake. In contrast, the higher degree of swelling observed for the electrospun membranes indicates the importance of membrane porosity in the water uptake process. However, a correlation for polymer concentration and water uptake for PCL-*L*-DTH membranes could not be established. The rationale proposed for such behavior is that PCL-*L*-DTH polyurethane membranes exhibit similar fiber diameters and porosity at all concentrations. As a result, the water uptake is constant. Jiang et al. have also observed a similar phenomenon in their studies with acrylonitrile based electrospun membranes [41]. In contrast, a the swelling kinetics for PCL-*C*-DTH membranes shows that the 10% (w/v) PCL-*C*-DTH membranes swelled significantly compared to the 15 and 20% membranes. The fiber diameter distribution (Fig. 4A–C) shows 10% PCL-*C*-DTH results in the formation of nanofibers as well as microfibers, but in contrast, polymer concentrations of 15 and 20% forms microfibers with average fiber diameters between 2200 and 2800 nm. An increase in the fiber diameter decreases the porosity of the membrane and the surface area that in turn decreases the swelling. However, swelling ratios of membranes obtained by electrospinning PCL-*C*-DTH solutions at 15 and 20% are somewhat higher than the swelling ratios exhibited by solvent cast PCL-*C*-DTH films (10% w/v). These results suggest the porous nature of the electrospun PCL-*C*-DTH, though hydrophobic, promotes water uptake.

Degradation study provides quantitative data on resistance of PCL-*L*-DTH and PCL-*C*-DTH against hydrolytic cleavage of the bonds present within the polymer backbone. Furthermore, these studies also provide an insight into the changes that occur in the surface morphology and the fiber diameters as the membranes degrade. Fig. 6A and B shows the initial degradation rates for all electrospun membranes are similar. In addition, a linear decrease in mass is observed as a function of time. Upon termination of the experiment, the mass losses for all membranes are quite similar. While the initial polymer concentration used for electrospinning does not seem to have an effect upon the mass loss properties, the membrane's morphologies are considerably altered. Following 4 weeks of degradation, the fibrous structure of 15% PCL-*L*-DTH membranes has completely disappeared and replaced by a congealed polymer structure. At higher PCL-*L*-DTH concentrations, parts of the initial fibrous structure are retained. However, the fibers are fused together at overlap junctions forming nodule-type structures. The fusion of fibers within the membranes possibly occurs due to a combination of mass loss (responsible for a reduction in the polymer intrinsic viscosity) and a low glass transition temperature (T_g) of PCL-*L*-DTH [42] (the glass transition temperature of non-degraded PCL-*L*-DTH (−39 °C) [23] being lower than the incubation temperature of 37 °C). A comparison of the mass loss characteristics of solvent cast films (10% w/v) and electrospun membranes shows films losing 10–12% mass over a period of 30 days. The mass loss for electrospun membranes is 18–20%. The higher mass loss of the electrospun membranes is likely due to a combination of several factors. The presence of a linear diisocyanate within the polymeric backbone permits the packing of soft segment chains and generates a partially phase-segregated semi-crystalline structure for dense films. However, these soft segment chains may align together, and the semi-crystalline structure of the material may be lost during electrospinning. Thus, these membranes are more amenable to

hydrolytic degradation. Finally, the electrospun membranes show a highly porous structure, which is absent in the case of dense films. The presence of a porous structure facilitates the entry of water and causes an increase in the degradation rate. PCL-*L*-DTH polyurethane is moderately hydrophobic, and studies performed by Sarkar et al. show that hydrolytic degradation of PCL-*L*-DTH primarily occurs via a surface erosion mechanism [23].

The degradation characteristics for PCL-*C*-DTH membranes mimic the PCL-*L*-DTH membranes. The electrospun membranes show a much higher mass loss (16–18%) compared to the solvent cast films (4–5%) in 4 weeks. The presence of a cyclic diisocyanate within the backbone of PCL-*C*-DTH prevents the packing and crystallization of the hard segments of the LTUs resulting in a predominantly amorphous polymer. The lack of crystallinity coupled with higher surface area, increased porosity, and the mechanism of hydrolytic degradation could result in degradation behavior similar to the one observed in the case of PCL-*L*-DTH electrospun membranes. These results are not surprising considering the similarity in the molecular structures and the physico-chemical properties of the two LTUs (barring the differences in the diisocyanate segment). While a number of similarities are observed in the degradation behaviors of the electrospun LTU membranes, more of the fiber structure is preserved for PCL-*C*-DTH membranes although with the loss of the porous structure. These differences between the two membranes could be related to the initial fiber diameter distributions where electrospinning PCL-*L*-DTH forms nanofibers but microfibers are obtained for PCL-*C*-DTH polyurethane.

5. Conclusions

Electrospun membranes have been formulated for the first time from two LTUs, PCL-*L*-DTH and PCL-*C*-DTH. Fiber sizes range from several hundred nanometers to a few micrometers and are influenced by the concentration of the polymer solutions. Generally, both the fiber diameters and their size distributions increase with concentrated polymer solutions. Although, bead formation is observed for PCL-*L*-DTH polyurethane at all concentrations, a clear correlation could not be ascertained. In contrast, uniform, bead free, and micron sized fibers are obtained for PCL-*C*-DTH. These differences in the morphology can be attributed to the differences in solution viscosities and eventually the chemical structures of the two polyurethanes. The porous structure of the electrospun membrane results in a larger degree of water absorption and an accelerated hydrolytic degradation compared to the solvent cast films [23]. While we expected polymer solution concentrations to have distinct effects on mass loss of electrospun membranes, no such correlations could be made based on the observed results. However, membranes spun at lower polymer concentrations show a considerable loss of fiber structure and fusion of the remaining fibers post-degradation.

Polyurethanes are important components for many FDA approved implantable devices. Since our membranes are elastic, biodegradable, and - fibrous, we believe tissue engineering is an ideal application for the LTUs since the structure produced by electrospinning mimics the extracellular matrix of natural tissues. These membranes could easily be modified for cellular attachment by either blending with collagen [43] or adsorbing fibronectin [44]. Furthermore, cytokines or DNA encoding for growth factors could be readily encapsulated within the scaffolds [36]. As LTU degrades, the controlled release of cytokines to the cells could accelerate cellular migration and enhance their attachment and function.

References

[1] Lamba NMK, Woodhouse KA, Cooper SL. Polyurethanes in biomedical applications. Boca Raton: CRC Press; 1998.
[2] Lelah MD, Cooper SL. Polyurethanes in medicine. Boca Raton: CRC Press; 1986.
[3] Gogolewski S. Colloid and Polymer Science 1989;267:757–85.
[4] Gogolewski S. In: Arshady R, editor. Desk reference of functional polymers. Syntheses and applications. Washington D.C.: American Chemical Society; 1996.
[5] Gogolewski S, Galletti G, Usia G. Colloid and Polymer Science 1987;265:774–8.
[6] Gogolewski S, Walpoth B, Rheiner P. Colloid and Polymer Science 1987;265:971–7.
[7] Gogolewski S, Pennings AJ. Makromolekulare Chemie – Rapid Communications 1983;4:675–80.
[8] Gogolewski S, Gorna K, Rahn B, Wieling R. In: Proceedings of the 27th Society for Biomaterials Annual Meeting, St. Paul; 2001. p. 573.
[9] Gogolewski S, Gorna K, Turner AS. In: Proceedings of the 48th Annual Meeting, Orthopaedic Research Society, Dallas; 2002. p. 10–13.
[10] Gogolewski S, Gorna K. Journal of Biomedical Materials Research, Part A 2006;79A:128–38.
[11] Guan J, Sacks MS, Beckman EJ, Wagner WR. Biomaterials 2004;25:85–96.
[12] Saad B, Neuenschwander P, Uhlschmid GK, Suter UW. International Journal of Biological Macromolecules 1999;25:293–301.
[13] Wang W, Ping P, Yu H, Chen X, Jing X. Journal of Polymer Science Part A: Polymer Chemistry 2006;44:5505–12.
[14] Borda J, Keki S, Bodnar I, Nemeth N, Zsuga M. Polymers for Advanced Technologies 2006;17:945–53.
[15] Gorna K, Gogolewski S. Journal of Biomedical Materials Research 2002;60:592–606.
[16] Santerre JP, Labow RS, Duguay DG, Erfle DJ, Adams GA. Journal of Biomedical Materials Research 1994;28:1187–99.
[17] Covolan VL, Di Ponzio R, Chiellini F, Fernandes EG, Solaro R, Chiellini E. Macromolecular Symposium 2004;218:273–82.
[18] Yeganeh H, Jamshidi H, Jamshidi S. Polymer International 2007;56:41–9.
[19] Guelcher SA, Gallagher KM, Didier JE, Klinedinst DB, Doctor JS, Goldstein AS, et al. Acta Biomaterialia 2005;1:471–84.
[20] Skarja GA, Woodhouse KA. Journal of Applied Polymer Science 2000;75:1522–34.
[21] Skarja GA, Woohouse KA. Journal of Biomaterials Science: Polymer Edition 2001;12:851–73.
[22] Sarkar D, Yang J-C, Lopina ST. Journal of Applied Polymer Science 2008;108:2345–55.
[23] Sarkar D. Development and characterization of L-tyrosine based polyurethanes for tissue engineering applications. Ph.D. dissertation, The University of Akron, Akron; 2007.
[24] Fromstein JD, Woodhouse KA. Journal of Biomaterials Science: Polymer Edition 2002;13:391–406.
[25] Riboldi SA, Sampaolesi M, Neuenschwander P, Cossu G, Mantero S. Biomaterials 2005;26:4606–15.
[26] Li C, Vepari C, Jin HJ, Kim HJ, Kaplan DL. Biomaterials 2006;27:3115–24.
[27] Lannutti J, Reneker D, Ma T, Tomasko D, Farson D. Materials Science & Engineering C 2007;27:504–9.
[28] Mengyan L, Mondrinos MJ, Gandhi MR, Ko FK, Weiss AS, Lelkes PI. Biomaterials 2005;26:5999–6008.
[29] Sen Gupta A, Lopina ST. Polymer 2004;45:4563–662.
[30] Sen Gupta A, Lopina ST. Journal of Polymer Science, Part A: Polymer Chemistry 2004;42:4906–15.
[31] Sarkar D, Yang JC, Sengupta A, Lopina ST. Journal of Biomedical Materials Research Part A, in press, doi:10.1002/jbm.a.32095.
[32] Sill TJ, von Recum HA. Biomaterials 2008;29:1989–2006.
[33] Ding B, Kim HK, Lee SC, Shao CL, Lee DR, Park SJ, et al. Journal of Polymer Science, Part B: Polymer Physics 2002;41:126–8.
[34] Lee KH, Kim HY, Khil MS, Ra YM, Lee DR. Polymer 2003;44:1287–94.
[35] Deitzel LM, Kleinmeyer J, Harris D, Beck Tan NC. Polymer 2001;42:261–72.
[36] Luu YK, Kim K, Hsiao BS, Chu B, Hadjiargyrou M. Journal of Controlled Release 2003;89:341–53.
[37] Boland ED, Wnek GE, Simpson DG, Pawlowski KJ, Bowlin GL. Journal of Macromolecular Science Part A: Pure and Applied Chemistry 2001;38:1231–43.
[38] Gu SY, Ren J. Macromolecular Materials and Engineering 2005;290:1097–105.
[39] Tripatanasuwan S, Zhong Z, Reneker DH. Polymer 2007;48:5742–6.
[40] Diez-Pena E, Quijada-Garrido I, Barrales-Rienda JM. Macromolecules 2002;35:8882–8.
[41] Wan LS, Xu ZK, Jiang HL. Macromolecular Bioscience 2006;6:364–72.
[42] Kim K, Yu M, Zong X, Chiu J, Fang D, Seo YS, et al. Biomaterials 2003;24:4977–85.
[43] Buttafoco L, Kolkman NG, Engbers-Buijtenhuijs P, Poot AA, Dijkstra PJ, Vermes I, et al. Biomaterials 2006;27:724–34.
[44] Nuttelman CR, Mortisen DJ, Henry SM, Anseth KS. Journal of Biomedical Materials Research 2001;57:217–23.